TDA Progress Report 42-115

November 15, 1993

Beam-Waveguide Antenna Servo Design Issues for Tracking Low Earth-Orbiting Satellites

W. K. Gawronski and J. A. Mellstrom

Ground Antennas and Facilities Engineering Section

Upcoming NASA missions will require tracking of low-orbit satellites. As a consequence, NASA antennas will be required to track satellites at higher rates than for the current deep space missions. This article investigates servo design issues for the 34-m beam-waveguide antennas that track low-orbit satellites. This includes upgrading the servo with a feedforward loop, using a monopulse controller design, and reducing tracking errors through either proper choice of elevation pinion location, application of a notch filter, or adjustment of the elevation drive amplifier gain. Finally, improvement of the signal-to-noise ratio through averaging of the oversampled monopulse signal is described.

I. Introduction

Future NASA missions will include low-orbiting satellites with significantly higher antenna tracking rates, as compared with the deep space missions. Thus, the JPL/NASA antenna servos should be upgraded to be able to follow commands at higher rates. A feedforward upgrade, discussed in [1], is the simple and reliable choice. For tracking, a monopulse controller is an alternative to the existing conscan tracking, since the former is much faster than the latter. The design and performance of a monopulse controller is discussed. It is shown that its performance can be improved through proper choice of the location of the elevation pinion, the implementation of a notch filter, or the adjustment of the amplifier gain. Finally, the improvement of the signal-to-noise ratio (SNR) of the monopulse signal is presented. By averaging the redundant monopulse samples, the SNR improvement is from 7 to 17 dB.

II. Feedforward Controller Design

Tracking accuracy of fast moving objects can be improved if a proportional-and-integral (PI) control system is augmented with a feedforward loop [1], shown in Fig. 1. In this diagram, G_p, G_c, G_f, and G_w denote transfer functions of the antenna's rate loop, PI controller, feedforward gain, and wind disturbance, respectively; r is a command; y is output (elevation and azimuth angles); e is tracking error in azimuth and elevation; u is plant input; and w is wind disturbance. Almost perfect tracking ($e \cong 0$) in the absence of disturbances is obtained for the feedforward gain G_f such that $G_f = j\omega I_2$, c.f., [1].

The closed-loop transfer function (elevation encoder to elevation command) for a system with and without the feedforward gain is compared in Fig. 2. The figure shows that for frequencies up to 1 Hz, the system with the feedforward gain has superior tracking properties as

$y = 0.5GHc + 0.5Gr$; and, since $G \cong I$ (see Eq. (5)), one obtains $y = 0.5(c + r)$.

The transfer function H of the monopulse controller is determined as follows. The monopulse bandwidth f_m is smaller than the encoder bandwidth f_o; therefore, the monopulse tracker will compensate for a slowly varying error signal e. If the condition presented in Eq. (6a) is satisfied for $f < f_m$, the monopulse tracking system will follow the command c. And since $G \cong I$ for $f < f_m$, $\| H \| \gg 1$ is required to satisfy the condition presented in Eq. (6a). In addition, a rapid roll-off rate for $f > f_m$ would be an advantage. However, the roll-off rate is limited through the Bode conditions, as specified in [6, p. 25]. Namely, the roll-off rate in the region of the gain crossover frequency must not exceed 40 dB/decade, and for a reasonable stability margin it must actually be smaller than this. Due to this restriction, the following transfer function of the monopulse tracker is chosen

$$H = \frac{2\pi f_m}{s} I_2 \tag{7}$$

This transfer function satisfies Eq. (6a) for $f < f_m$ and has a roll-off rate of 20 dB/decade for $f > f_m$ (see Fig. 5). The parameter f_m of H is determined by analyzing the root locus of the monopulse closed-loop system with respect to f_m. The plot of real parts of closed-loop poles is shown in Fig. 6. It shows that for $f_m \geq 0.067$ Hz, the monopulse system is unstable. In order to maintain a reasonable stability margin, $f_m = 0.04$ Hz is chosen.

The plant transfer function G is obtained for the DSS-13 antenna with the encoder loop closed and the feedforward loop implemented. The magnitudes of the plant transfer function are shown in Fig. 7. From the figure, one can see that the condition of Eqs. (5a) and (5b) are satisfied, but the condition of Eq. (5c) is violated for some frequencies from the interval $f = [2, 10]$ Hz. This violation will cause some performance deterioration.

The azimuth and elevation components of the command signal r are shown in Fig. 3. The command c is slightly deviated from r by δ, i.e., $c = r + \delta$, where $\| \delta \| \ll \| r \|$. The plot of δ is shown in Fig. 8. Magnitudes of the transfer functions are shown in Fig. 9 from input r to output y, and in Fig. 10 from input c to output y. For the case of $\delta = 0$, the same input c and r are obtained and denoted u, i.e., $c = r = u$. In this case, one obtains from Eq. (3) $y = G_o u$, where $G_o = G_c + G_r$. The plots of the magnitudes of G_o are shown in Fig. 11. They indicate that the system follows low-frequency command c, high-frequency command r, and low- and high-frequency command u.

Implementation of the monopulse controller requires its discretization in time. The monopulse signal is supplied with the rate f_d Hz or with the sampling time $T = 1/f_d$ sec. In the case of the DSS-13 antenna, the sampling rate is 10 Hz. A block diagram of the discrete-time monopulse tracker is shown in Fig. 12. The main difference between the continuous-time and the discrete-time trackers lies in a delay of the tracking error.

The monopulse closed-loop systems with sampling rates of 10 and 50 Hz have been simulated. The 50-Hz sampled system has been simulated for evaluation of accuracy of the slower, sampled 10-Hz system. The simulations show similar results for 10- and 50-Hz sampling and are shown in Fig. 8 for the 10-Hz sampled system, where the solid line denotes the tracking error, e, and the dashed line the deviation, δ. The plots show that the pointing accuracy increased more than twofold in both cases. A sampling rate of 10 Hz is satisfactory to maintain the accuracy of the control system, and the 0.1-sec delay does not deteriorate the system performance.

IV. Improving Tracking Performance

As mentioned before, the implementation of the feedforward loop causes a significant excitation of flexible motion of the antenna, specifically in the elevation loop. The mode of deformation for the highest peak in the elevation-to-elevation transfer function is shown in Fig. 13. It is a bending mode of the antenna structure, strongly excited not only by the elevation command but also by the azimuth command. It impacts the stability and performance of an antenna. This mode is extremely difficult to control with elevation and/or azimuth torques, but any one of the following measures can be taken to reduce the impact of this mode on tracking performance: proper location of the elevation pinion, application of a notch filter, or adjustment of the amplifier gain in elevation drive. These measures are described below.

A. Choosing the Elevation Pinion Location

The antenna dynamics for the three positions of the elevation pinion, $\alpha = 0$, 60, and 90 deg, as shown in Fig. 14, have been simulated. The step responses are presented in Fig. 15, showing increased damping of transient motion for the higher location of the pinion. In consequence, the monopulse gains can be increased for the higher pinion, causing smaller tracking errors, as shown in Table 1. The decrease is almost proportional to $\cos\alpha$, which can be explained by the fact that the bending mode is excited mainly by the horizontal component F_h of the elevation pinion force F_t, proportional to the $\cos\alpha$, c.f., Fig. 14.

where P_s and P_n are signal and noise powers, respectively. The noise impacts the pointing accuracy of the control system. Here a simple method that improves SNR is discussed.

The monopulse signal $u(i\Delta t)$ (see Fig. 24) consists of a true measurement $u_o(i\Delta t)$ and a noise $n(i\Delta t)$

$$u(i\Delta t) = u_o(i\Delta t) + n(i\Delta t) \tag{12}$$

where $u_o(i\Delta t) = y_o(i\Delta t) - y(i\Delta t)$. It is assumed initially that the noise $n(i\Delta t)$ is a white noise with zero mean, $E(n(i\Delta t)) = 0$, where $E(.)$ is the expectation operator. The assumption is the worst-case scenario. White noise consists of components of all frequencies of equal intensity s_o, up to the Nyquist frequency f_c, as in Fig. 25(a). Typically, the measurement noise is rather a high-frequency noise; thus its impact on system performance is less severe than that of the white noise.

The monopulse signal $u(i\Delta t)$, shown in Fig. 26 for sampling time $\Delta t = 0.02$ sec, is transmitted to the antenna controller in clusters every N samples (typically $N = 5$); thus the new sampling period is

$$\Delta T = N\Delta t \tag{13}$$

and a cluster $U(i\Delta T) = \{u_1(i\Delta T), u_2(i\Delta T), \cdots, u_N(i\Delta T)\}$, consists of N measurements $u_k(i\Delta T)$

$$u_k(i\Delta T) = u(i\Delta T + k\Delta t),\ k = 1, \cdots, N \tag{14}$$

The mean value, $m_k = E(u_k(i\Delta t))$, and the variance, $\sigma_k = E(\Delta u_k(i\Delta T))^2$, of each component are the same in the cluster

$$m_k = m_N,\ \sigma_k^2 = \sigma_N^2,\ k = 1, \cdots, N \tag{15}$$

This assumption has the following meaning: the value of $u_o(i\Delta t)$ is considered constant within the period ΔT if the reaction of the antenna to $u_o(t_o + i\Delta t)$ is the same as to $u_o(t_o + N\Delta t)$ for $i = 1, \cdots, N$. This property has been confirmed by the earlier simulations reported in [1].

Although the monopulse signal is sent to the controller in clusters, only the last component, $u_N(i\Delta T) = u(i\Delta T + N\Delta t)$, is used to drive the monopulse controller. This excess information is used to reduce the signal-to-noise ratio by averaging the signal within a cluster. The average value, $u_{av}(i\Delta T)$, of the monopulse signal within the cluster of N samples is obtained

$$u_{av}(i\Delta T) = \frac{1}{N}\sum_{k=1}^{N} u_k(i\Delta T) \tag{16}$$

It is shown in the Appendix that in the case of white noise the mean value (m_{av}) of the averaged process, $u_{av}(i\Delta T)$, and the mean value (m_N) of the nonaveraged process, $u_N(i\Delta T)$, are the same, while the variance of the averaged process (σ_{av}^2) is smaller than the variance of the nonaveraged process (σ_N^2) by the factor N

$$m_{av} = m_N,\ \sigma_{av}^2 = \frac{\sigma_N^2}{N} \tag{17}$$

Define r_s, the ratio of variances of nonaveraged and averaged signals, as

$$r_s = \frac{\sigma_N^2}{\sigma_{av}^2} \tag{18a}$$

and its logarithmic counterpart, an SNR increase, ΔSNR, as

$$\Delta SNR = SNR_{av} - SNR = 10\log_{10} r_s \text{ dB} \tag{18b}$$

Then, for white noise, from the definition in Eq. (11), one obtains $r_s = N$ and $\Delta SNR = 10\log_{10} N$ dB.

Consider high-frequency noise with a constant spectrum within the interval $[f_o,\ f_c]$ (see Fig. 25(b)) such that $0 < f_o < f_c$, f_o is a cutoff frequency (the lowest frequency component of the noise), and f_c is the Nyquist frequency, $f_c = 0.5/\Delta t$. Results of noise reduction for the high-frequency noise, obtained through simulations, are shown in Fig. 27. From this plot of the ratio, r_s, versus cutoff frequency, f_o, it is evident that the high-frequency noise is more suppressed through averaging than is the white noise (r_s increases from 5 in the case of white noise to 50 in the case of high-frequency noise for cutoff frequencies of 8 Hz and higher, and SNR increase, ΔSNR, is from 7 to 17 dB, respectively). These results have also been confirmed by simulations of monopulse tracking with $SNR = 20$ dB, where the elevation pointing error for the

Table 1. Pointing errors.

Pinion position, deg	Elevation errors, mdeg	Cross-elevation errors, mdeg	Total errors, mdeg
0	1.43	0.14	1.44
60	0.76	0.08	0.77
90	0.35	0.07	0.36

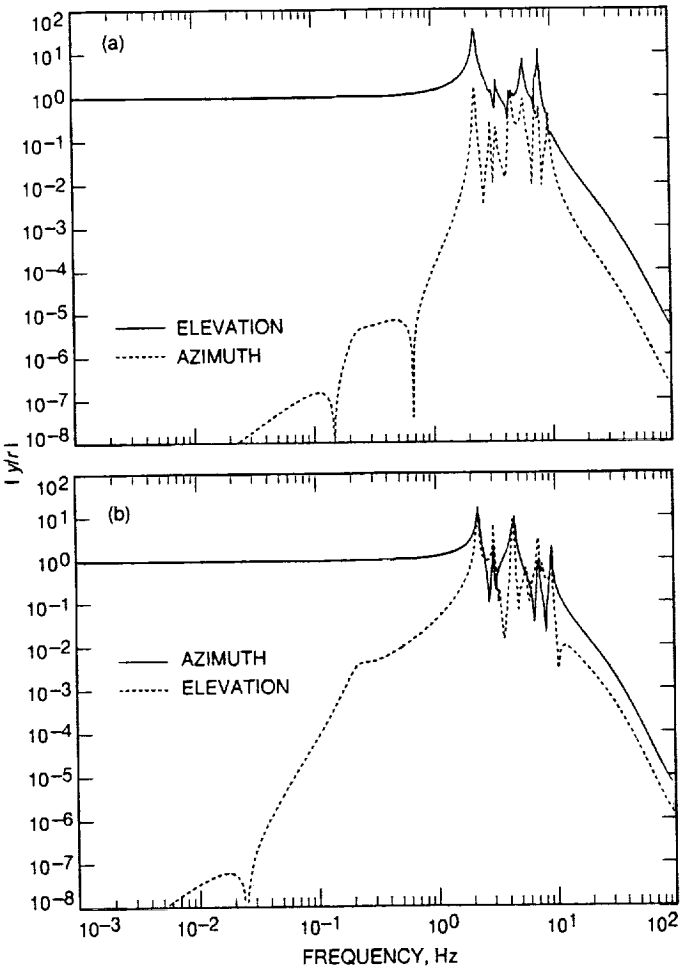

Fig. 7. Magnitudes of the plant transfer function from input r to output y: (a) elevation angle command and (b) azimuth angle command.

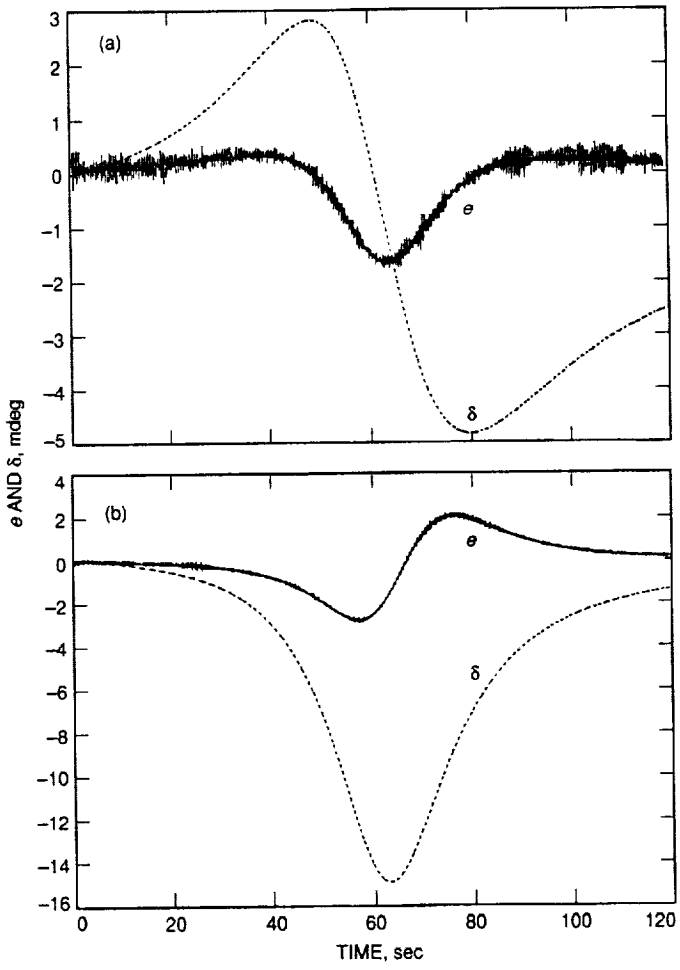

Fig. 8. Tracking error e and deviation δ in (a) elevation and (b) azimuth.

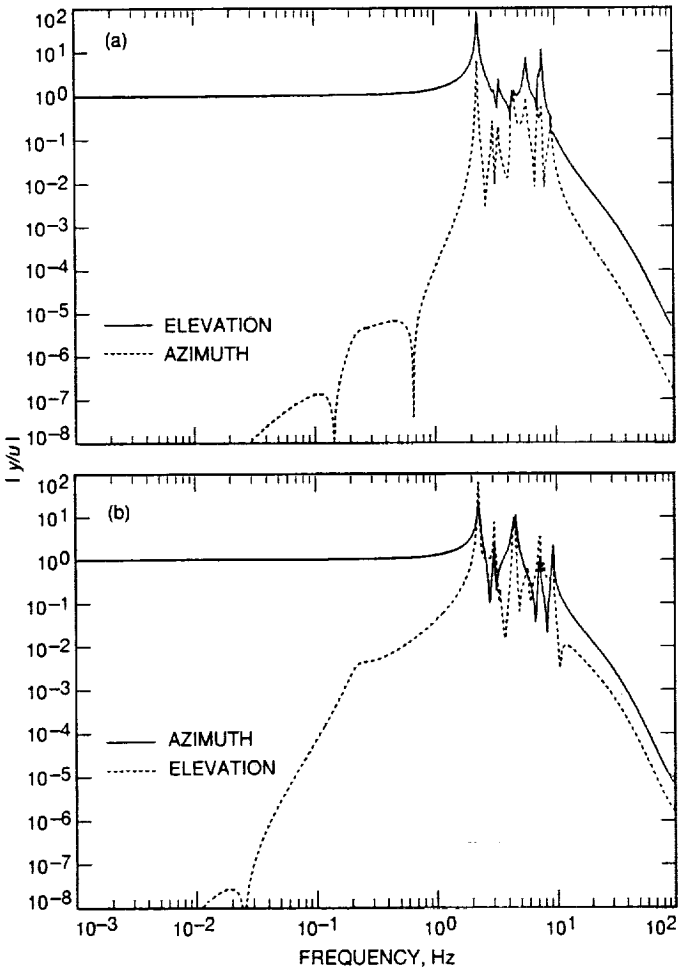

Fig. 11. Magnitudes of the closed-loop transfer function from input $u = c = r$ to output y: (a) elevation angle command and (b) azimuth angle command.

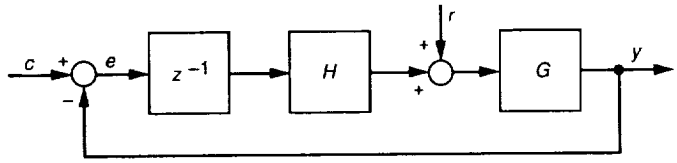

Fig. 12. The discrete-time monopulse tracking system.

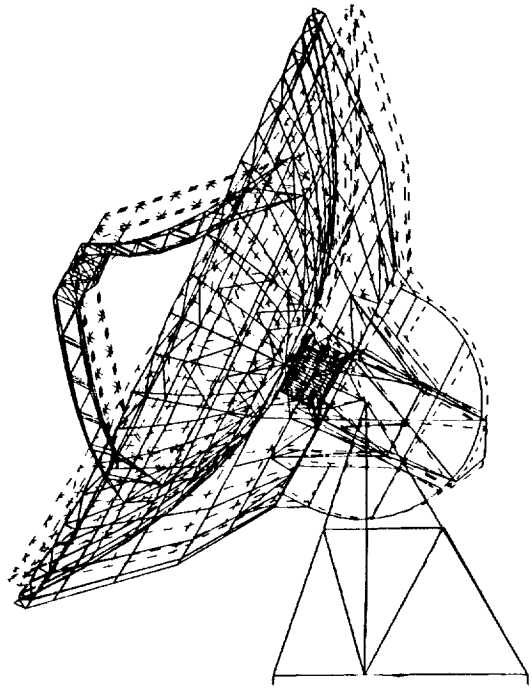

Fig. 13. The bending mode of the antenna.

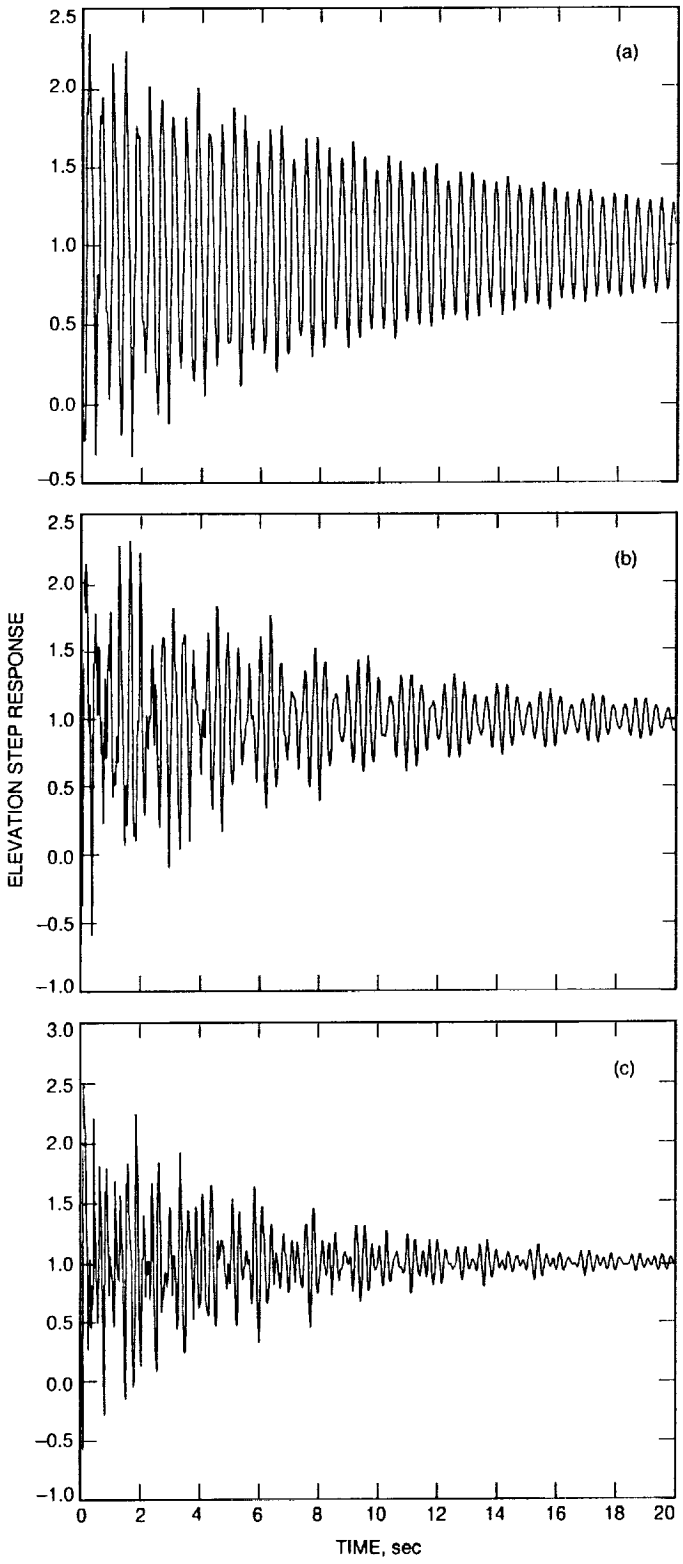

Fig. 15. Step responses (elevation command to elevation encoder) of the closed-loop system, for the elevation pinion at: (a) 0, (b) 60, and (c) 90 deg.

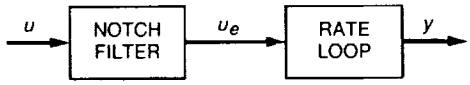

Fig. 16. The rate loop model with a notch filter.

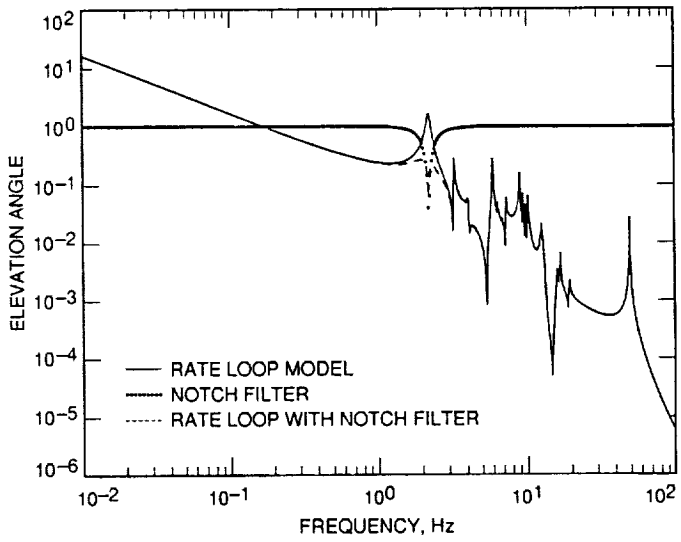

Fig. 17. Transfer functions.

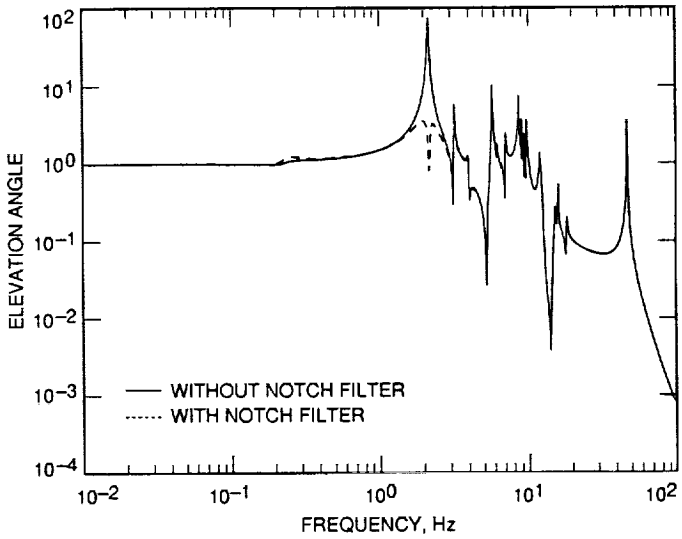

Fig. 18. Transfer functions (elevation command to elevation encoder) of the closed-loop antenna.

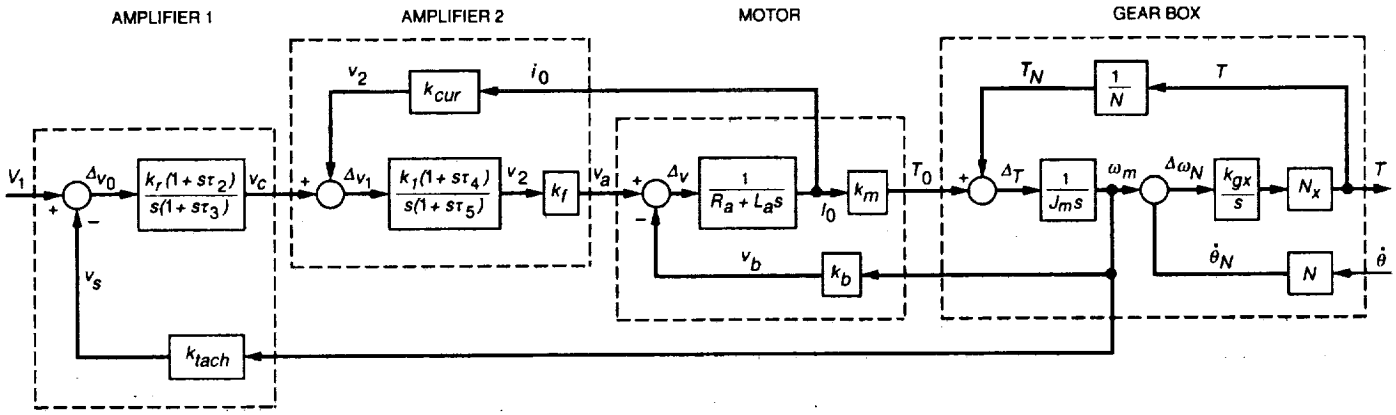

Fig. 21. The elevation drive model.

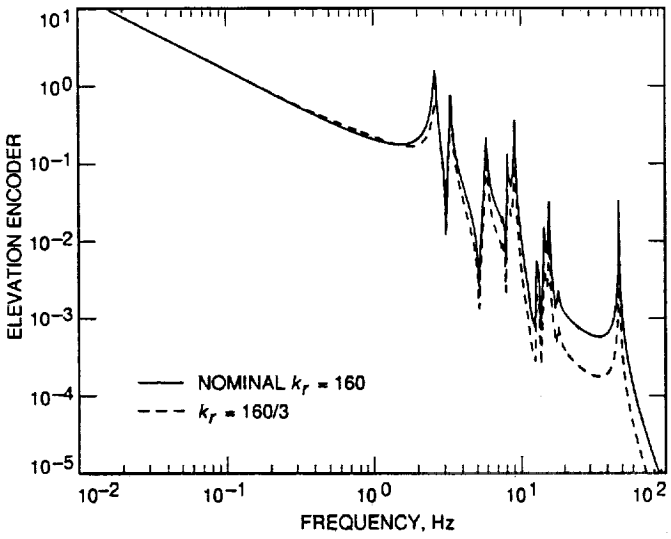

Fig. 22. Transfer functions (elevation rate command to elevation encoder) of the rate loop model.

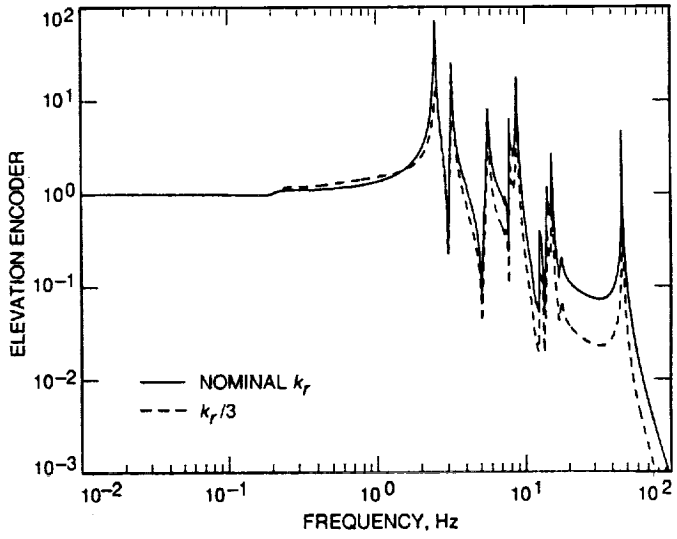

Fig. 23. Transfer functions (elevation command to elevation encoder) of the closed-loop antenna.

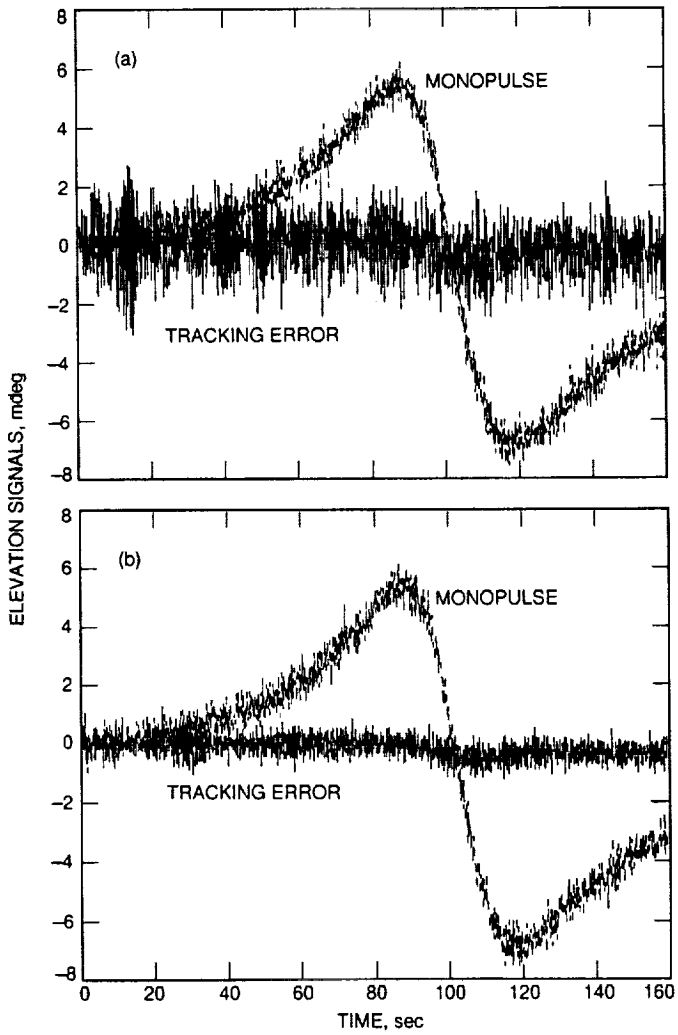

Fig. 28. Elevation tracking error and noisy monopulse signal (a) without averaging and (b) with averaging.